

Chiral condensate and the Equation Of State at non-zero baryon density from hadron resonance gas model with repulsive mean-field

Deeptak Biswas,^{1,2} Peter Petreczky,³ and Sayantan Sharma¹

¹*The Institute of Mathematical Sciences, a CI of Homi Bhabha National Institute, Chennai, 600113, India*

²*School of Physical Sciences, National Institute of Science Education and Research,
An OCC of Homi Bhabha National Institute, Jatni-752050, India*

³*Physics Department, Brookhaven National Laboratory, Upton NY 11973, USA*

We study the QCD equation of state and the chiral condensate using the hadron resonance gas with repulsive mean-field interactions. We find that the repulsive interactions improve the agreement with the lattice results on the derivatives of the pressure with respect to the baryon chemical potential up to eighth order. From the temperature dependence of the chiral condensate we estimate the crossover temperature as a function of baryon chemical potential, $T_c(\mu_B)$. We find that the chiral crossover line starts to deviate significantly from the chemical freeze-out line already for $\mu_B > 400$ MeV. Furthermore, we find that the chiral pseudo-critical line can be parameterized as $T_c(\mu_B)/T_c(0) = 1 - \kappa_2(\mu_B/T_c(0))^2 - \kappa_4(\mu_B/T_c(0))^4$ with $\kappa_2 = 0.0150(2)$ and $\kappa_4 = 3.1(6) \cdot 10^{-5}$ which are in agreement with lattice QCD results for small values of μ_B . For the first time we find a tiny but non-zero value of κ_4 in our study.

I. INTRODUCTION

Understanding QCD matter at non-zero temperatures and baryon densities presents several challenges on the theory side. Apart from asymptotically large temperatures and baryon densities when perturbation theory can make predictions for thermodynamics, the problem is non-perturbative. For zero baryon density, lattice QCD methods have provided continuum extrapolated results for physical quark masses for many thermodynamic quantities. However, due to the infamous *sign-problem*, the lattice Monte Carlo techniques based on the method of important sampling break down at finite densities. Attempts to extend the lattice QCD calculations to non-zero baryon densities through Taylor expansion in baryon chemical potential, μ_B , or imaginary chemical potential approach has allowed us to understand QCD thermodynamics $\mu_B < 2.5 T$ [1–4], which can be extended in a certain temperature regime to $\mu_B/T \sim 3.5$ [5].

Below the chiral crossover temperature, QCD thermodynamics can be fairly well understood using the Hadron Resonance Gas (HRG) model. The main idea of this model is that the interactions between hadrons can be taken into account through hadronic resonances and the interacting gas of hadrons can be replaced by a gas of non-interacting hadrons and hadronic resonances treated as stable particles. This approach can be justified within the framework of relativistic virial expansion [6, 7] and the comparison between the HRG model results and the lattice data [8–13]. Indeed, the most recent lattice QCD calculations of the QCD pressure and the second order fluctuations and correlations of conserved charges agree well with the the HRG model results [2, 14–18]. For some quantities like baryon-strangeness or baryon-charm correlations, it is important to include additional hadron states that are not listed in the Particle Data Group (PDG) but are predicted by lattice QCD and quark models [18–21]. For strangeness-baryon number correlation, this idea is further supported by the calculation within the relativistic virial expansion with state-of-the-art phase shift analysis [22].

The temperature dependence of the chiral condensate has been studied within the HRG model [23–27] and attempts to use the HRG model to estimate the chiral crossover temperature at small baryon density have been made recently [27]. There is a widespread expectation that the chiral crossover may become a true phase transition at large baryon density, namely that the crossover will turn into a first-order phase transition at $\mu_B = \mu_B^{CEP}$ corresponding to the critical end-point (CEP). Lattice QCD results strongly disfavor $\mu_B^{CEP} < 400$ MeV for a range of temperatures around $0.85 T_c$ while functional renormalization group studies estimate μ_B^{CEP} to be even larger, around 635 MeV [28] at $T = 107$ MeV. Therefore, it would be interesting to estimate the chiral crossover temperature at larger values of baryon density using the HRG model framework.

The agreement between lattice QCD and the HRG model results no longer holds for higher order fluctuations of conserved charges [2–4, 29]. This may highlight the importance of the inclusion of non-resonant attractive interactions as well as repulsive interactions among the baryons, which could become very important at higher baryon densities. The most common approach to include repulsive interactions within the HRG model is through the inclusion of a hard-core repulsive excluded volume for hadrons [30–37]. Recently these models have been refined to include both repulsive and attractive non-resonant interactions via a Van der Waals-like potential [38–42]. Another approach to include the repulsive interactions is through the mean-field approximation. Here the strength of the repulsive interaction is proportional to the baryon density [43–45]. It has been shown that this model can explain the deviations from the HRG model seen in the lattice QCD calculations of higher-order derivatives of the QCD pressure with respect to the

baryon chemical potential [46]. Following this work the use HRG model with repulsive mean-field interactions has been explored for explaining the lattice results on the QCD equation of state [47, 48] and fluctuations and correlations of conserved charges [49, 50].

The aim of this paper is to study the temperature and the μ_B -dependence of the chiral condensate, and using this to estimate the chiral crossover temperature as a function of μ_B . We will also revisit the description of the higher-order baryon number fluctuations and the QCD equation of state within the HRG model with repulsive mean-field interactions in the light of the newest lattice QCD results. The paper is organized as follows: In the next section, we review the HRG model with repulsive interactions. In this section, we also present the comparison of this model with the state of the art lattice QCD results on fluctuations of conserved charges. In section III we discuss the calculation of the chiral condensate as a function of temperature and baryon chemical potential. In section IV we present our results e.g., the estimate of the chiral crossover temperature as a function of baryon chemical potential, curvature of the pseudo-critical line. In section V, we discuss the temperature and baryon density dependence of the speed of sound for the strangeness neutral system. Finally, our conclusions are presented in section VI. In the Appendices, we give some technical details of the calculations.

II. REPULSIVE BARYON INTERACTIONS WITHIN HRG MODEL

The pressure for an interacting ensemble of baryons and anti-baryons with densities n_b and $n_{\bar{b}}$ respectively can be represented within the mean-field approximation as [48, 49],

$$P_{int}^{B\{\bar{B}\}} = T \sum_{i \in B\{\bar{B}\}} \int g_i \frac{d^3 p}{(2\pi)^3} \ln \left[1 + e^{-\beta(E_i - \mu_{eff})} \right] + \frac{K}{2} n_{b\{\bar{b}\}}^2. \quad (1)$$

Here the effective chemical potential for the i^{th} species is defined as $\mu_{eff} = B_i \mu_B - K n_{b\{\bar{b}\}}$, with B_i is the baryon number of the baryons, $B_i = +1$, and anti-baryons, $B_i = -1$, and $\beta = 1/T$, where T is the temperature of this system. The number densities for baryons and anti-baryons can be solved self-consistently from the following pair of equations,

$$n_b = \sum_{i \in B} \int g_i \frac{d^3 p}{(2\pi)^3} \frac{1}{e^{\beta(E_i - \mu_B + K n_b)} + 1} \quad \text{and} \quad n_{\bar{b}} = \sum_{i \in \bar{B}} \int g_i \frac{d^3 p}{(2\pi)^3} \frac{1}{e^{\beta(E_i + \mu_B + K n_{\bar{b}})} + 1}. \quad (2)$$

The total pressure within the HRG model is the sum of the contributions from this interacting ensemble of the (anti)baryons and the non-interacting ensemble of mesons. We include the quark model (QM) predicted states [51, 52] in addition to the Particle Data Group (PDG) listed hadrons up to mass 3 GeV [53]. We denote this HRG model with the extended list of particles as the QMHRG model. For the $\mu_B = 0$ we can use the Boltzmann approximation for baryons and anti-baryons due to their large masses. Therefore, for the pressure and the number density we could write the following set of equations [46]:

$$P_{int} = T(n_b + n_{\bar{b}}) + \frac{K}{2}(n_b^2 + n_{\bar{b}}^2) \quad \text{and} \quad n_{b\{\bar{b}\}} = \sum_{i \in B\{\bar{B}\}} \int g_i \frac{d^3 p}{(2\pi)^3} e^{-\beta(E_i - \mu_{eff})} \quad (3)$$

This approximation greatly simplifies the calculations of the baryon number susceptibilities, which are defined as

$$\chi_B^n = \frac{\partial^n [P(\mu_B/T)/T^4]}{\partial (\mu_B/T)^n}, \quad n = 2, 4, 6, 8 \quad (4)$$

The explicit expressions of χ_n^B are presented in Appendix A. In this work, we have included the partial pressures of the QMHRG states with repulsive interactions among the (anti) baryons at the mean-field level. Typically in the earlier works, the mean-field coefficient has been chosen to be $K = 450 \text{ MeV fm}^3$ which is equivalent to 56.25 GeV^{-2} [46, 54] from phenomenological considerations. Here we suggest a new way of estimating this constant. Our approach is motivated by the fact that we have high precision lattice QCD data for χ_2^B and χ_4^B extrapolated to the continuum limit [4, 18, 29]. Therefore, we adjust the value of K to reproduce these lattice QCD results. In Fig. 1 we show the comparison of our results for the second and fourth order baryon number fluctuations with the corresponding lattice QCD results. The lattice QCD results on χ_2^B results disagree with the QMHRG model results for $T > 150 \text{ MeV}$, while the lattice QCD results for χ_4^B start to disagree with QMHRG model results already for $T > 140 \text{ MeV}$, when no repulsive interactions are taken into account. By including repulsive mean-field interactions within the QMHRG model with $K = 33 \text{ GeV}^{-2}$, we obtain a good agreement with the lattice QCD results for both χ_2^B and χ_4^B up to $T \sim 155 \text{ MeV}$.

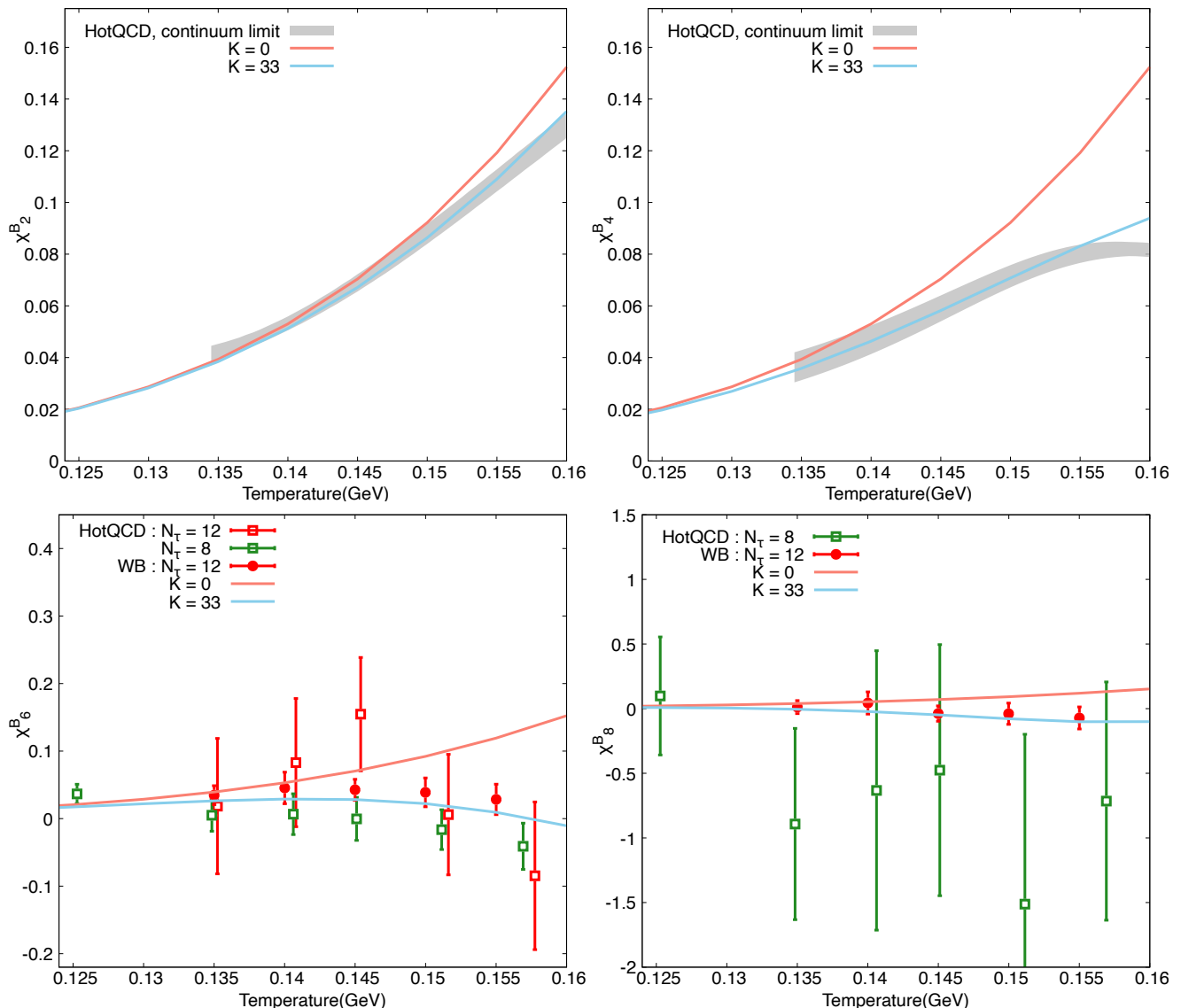


FIG. 1. The second (top left), fourth (top right), sixth (bottom left), and eighth (bottom right) order baryon number fluctuations results compared between ideal QMHRG (red line), mean-field QMHRG (blue line) models and lattice QCD results with physical quark masses. Lattice results for $N_\tau = 12$ and $N_\tau = 8$ are shown as red and green points respectively with the squares representing HotQCD [55] results and the circles corresponding to Wuppertal-Budapest (WB) results [2]. The gray bands represent the fluctuation data in the continuum limit from the HotQCD collaboration [55].

Unfortunately there are no published continuum extrapolated lattice results for sixth and eighth-order baryon number fluctuations. There are lattice QCD results for $N_\tau = 8$ and $N_\tau = 12$ from the HotQCD collaboration [55] and $N_\tau = 12$ results from the Wuppertal-Budapest Collaboration [2]. Here N_τ is the temporal lattice extent that is related to the temperature and the lattice spacing a , as $N_\tau = 1/(aT)$. In the lower panels of Fig. 1 we show the comparison of the QMHRG model results with the corresponding lattice QCD results for χ_6^B and χ_8^B . We see from the figure that the QMHRG model results with repulsive mean-field and $K = 33 \text{ GeV}^{-2}$ agree well with the lattice QCD results for χ_6^B and χ_8^B within errors. The agreement with Wuppertal-Budapest lattice results is especially remarkable as these results have relatively small errors. These lattice QCD results clearly disagree with the QMHRG model without repulsive interactions, see Fig. 1 (lower panels). We thus conclude that in order to apply the QMHRG model at large values of baryon number density to describe QCD, repulsive baryon-baryon interactions have to be taken into account.

In the above discussion, we assumed that both baryons and baryon resonances contribute equally to the mean-field. This is certainly a very simplistic assumption. One may expect that not all baryon resonances contribute to the mean-field at the same level because of their short life times. As an extreme assumption, we can assume that only

ground state baryons contribute to the repulsive mean-field. As shown in Appendix A, we can describe the lattice results on χ_2^B , χ_4^B , χ_6^B and χ_8^B also in this case if the parameter K is increased from $K = 33 \text{ GeV}^{-2}$ to $K = 100 \text{ GeV}^{-2}$. We also calculated the QCD pressure and energy density using the QMHRG model with repulsive mean-field interaction. We find that repulsive mean-field interaction has a significant effect on the pressure and energy density for $\mu_B/T \leq 2$, and its inclusion improves the agreement with the lattice QCD data. This is shown in the Appendix B. We will return to the calculations of the equations of state within the QMHRG model with repulsive interactions in section IV D for a strangeness neutral system.

III. CHIRAL CONDENSATE IN THE MEAN-FIELD QMHRG MODEL

The light quark condensate, at non-zero temperature and density is defined as,

$$\langle \bar{\psi}\psi \rangle_{l,T} = \langle \bar{\psi}\psi \rangle_{l,0} + \frac{\partial P}{\partial m_l}, \quad (5)$$

where m_l is the light quark mass and P is the pressure of the thermodynamic medium described by QCD. We work with two degenerate light quarks, $m_u = m_d = m_l$. In the HRG model, the derivatives of the pressure with respect to the light quark mass can be written as the mass derivative of the interacting baryonic gas pressure and the ideal mesonic gas pressure. Using Eqs. 1 and 2 the derivative of the interacting baryonic pressure in Eq. 1 can be further written as,

$$\left(\frac{\partial P_{int}}{\partial m_l} \right) = - \sum_{i=B} M_i \frac{\partial M_i}{\partial m_l} \int g_i \frac{d^3 p}{(2\pi)^3} \frac{f_i^b}{E_i} - \sum_{i=\bar{B}} M_i \frac{\partial M_i}{\partial m_l} \int g_i \frac{d^3 p}{(2\pi)^3} \frac{f_i^{\bar{b}}}{E_i}. \quad (6)$$

Here $f_i^{b\{\bar{b}\}}$ is the Fermi-Dirac distribution function corresponding to the baryons and anti-baryons with the modified chemical potential $\mu_{eff} = B_i \mu_i - K n_{b\{\bar{b}\}}$. In the limit, $K = 0$ one obtains the ideal gas result of Ref. [27]. The calculations of the mass derivative of the mesonic pressure are the same as in Ref. [27].

The non-trivial input needed for the calculation of the chiral condensate is the dependence of the hadron and resonance masses on the light quark mass m_l . In this work, we have estimated these mass derivatives following Ref. [27]. The uncertainties in the derivatives of the hadron masses with respect to m_l have been estimated in Ref. [27], and we propagate these uncertainties when evaluating the temperature and μ_B -dependence of the chiral condensate. As in our previous work, we use the renormalized chiral condensate defined by the HotQCD collaboration [56] as,

$$\Delta_R^l = d + m_s r_1^4 [\langle \bar{\psi}\psi \rangle_{l,T} - \langle \bar{\psi}\psi \rangle_{l,0}], \quad (7)$$

where the parameter r_1 is derived from the static quark potential [57] and $d = r_1^4 m_s (\lim_{m_l \rightarrow 0} \langle \bar{\psi}\psi \rangle_{l,0})^R$. In the chiral limit, the light quark condensate has only a multiplicative renormalization factor. The superscript R denotes the renormalized quantity. Taking into account the fact that $(\lim_{m_l \rightarrow 0} \langle \bar{\psi}\psi \rangle_{l,0})^R = 2\Sigma$ and using the values of the low energy constant of $SU(2)$ chiral perturbation theory (χ_{PT}), $\Sigma^{1/3} = 272(5) \text{ MeV}$ and $m_s = 92.2(1.0) \text{ MeV}$ in $\overline{\text{MS}}$ scheme at $\mu = 2 \text{ GeV}$ from the FLAG 2022 review for 2+1 flavor case [58], as well as $r_1 = 0.3106 \text{ fm}$ [59], we obtain the value of $d = 0.022791$.

We estimate the chiral crossover temperature, T_c as the temperature where the renormalized chiral condensate drops to half of its vacuum value. From the lattice QCD calculations at $\mu_B = 0$ we know that this definition of the chiral crossover temperature agrees well with the usual definition of the chiral crossover temperature, defined as the peak position of the chiral susceptibility [56]. In our previous work, we showed that using this definition of T_c and the temperature dependence of Δ_l^R within QMHRG model, one obtains a value of T_c at $\mu_B = 0$ as well as for small values of μ_B , which is only a few MeV larger than the lattice results [27]. We expect that the above criterion to estimate T_c should work at larger values of μ_B as long as we are far away from a true phase transition. Therefore, in this work, we assume that the chiral transition remains a crossover transition also for large values of μ_B and estimate the chiral crossover temperature using QMHRG model and the above considerations. This is reasonable since there is no definite indication from lattice QCD for a true phase transition at large μ_B , and based on symmetry arguments the transition could be a crossover even for very large values of μ_B [60].

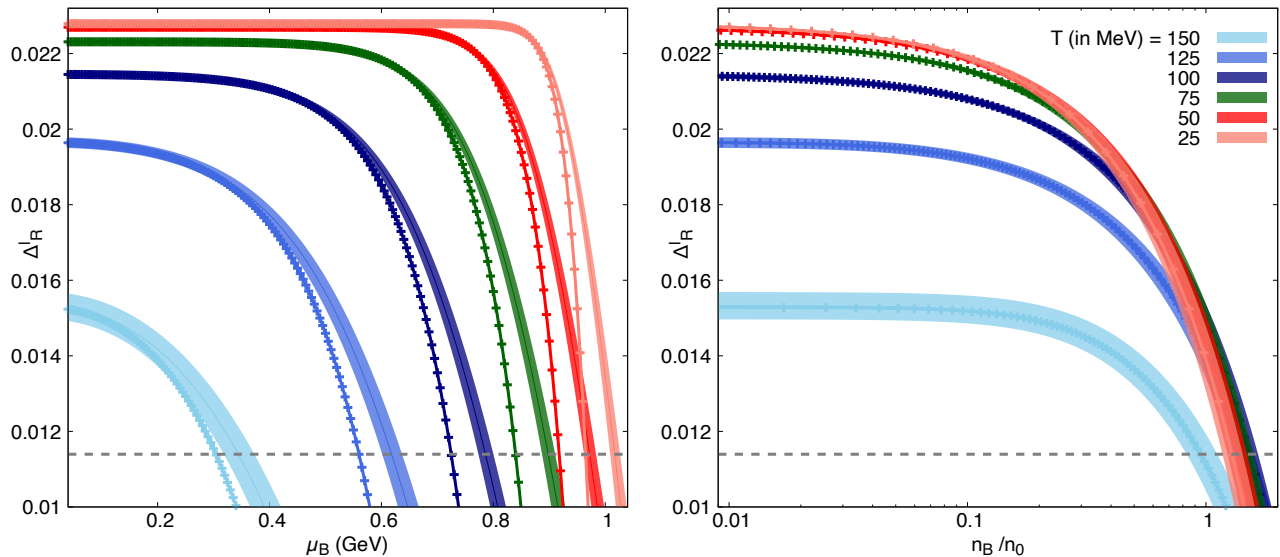


FIG. 2. (Left) The μ_B -dependence of the renormalized chiral condensate at different temperatures $T = 25$ -150 MeV. The bands are results from the QMHRG model with repulsive mean-field interaction and the lines with points are the results from the ideal QMHRG model. (Right) The variation of the Δ_R^l with net-baryon number density normalized by the nuclear saturation density, $n_0 = 0.16 \text{ fm}^{-3}$ for the same range of temperatures. The width of the bands represents the uncertainty of the chiral condensate due to the uncertainties in the quark mass derivatives of the hadron masses, see text for details.

IV. RESULTS ON THE CHIRAL CROSSOVER LINE

A. Renormalized chiral condensate in the mean-field formalism:

One of the goals of this study is to study the dependence of the renormalized chiral condensate on temperature and baryon chemical potentials for a large range of μ_B , including values not accessible in lattice QCD calculations. With the already estimated value of the mean-field parameter $K = 33 \text{ GeV}^{-2}$, we have evaluated Δ_R^l as a function of μ_B for different temperatures, shown in Fig. 2. We have also shown the Δ_R^l calculated in the non-interacting QMHRG model for comparison. In the figure, the uncertainty in the values of renormalized chiral condensate obtained in QMHRG model with repulsive mean-field interactions due to the uncertainties of the quark mass derivatives, is represented as a width of the lines. For the non-interacting QMHRG model, we do not show the corresponding uncertainties for better visibility. For temperatures $T < 100 \text{ MeV}$, we observe a prominent plateau in the value of Δ_R^l for a range of baryon chemical potentials, the extent of which reduces with increasing temperature. Furthermore, we observe that the renormalized condensate falls faster with increasing μ_B from the plateau region for the non-interacting QMHRG model compared to the QMHRG with repulsive mean-field interactions. Thus the repulsive mean-field pushes the transition point toward larger values of μ_B . As stated above we use the condition of the chiral condensate dropping to half of its vacuum values to estimate the crossover point. Thus using the values of μ_B where Δ_R^l is at half of its vacuum value for each temperature we obtain the estimate of crossover line as a function of baryon chemical potential, $T_c(\mu_B)$.

We are also interested in estimating the chiral crossover temperature as a function of the net baryon density, n_B . Therefore, we have also studied the dependence of Δ_R^l on n_B . The right panel of Fig. 2 shows the change in Δ_R^l at different temperatures as a function of net baryon number density n_B scaled by the nuclear saturation density $n_0 = 0.16 \text{ fm}^{-3}$. At a fixed temperature, Δ_R^l decreases as the net baryon density increases because baryons significantly contribute to the reduction of the chiral condensate. From this figure, we observe that the density corresponding to the chiral crossover transition for $T = 100 \text{ MeV}$ slightly exceeds that for $T = 25 \text{ MeV}$, for example. This seemingly contradicts the usual expectation that n_B decreases as T increases along the chiral crossover line. This is an artifact of the hadron resonance gas model at very low temperatures, as discussed in Sec. IV C.

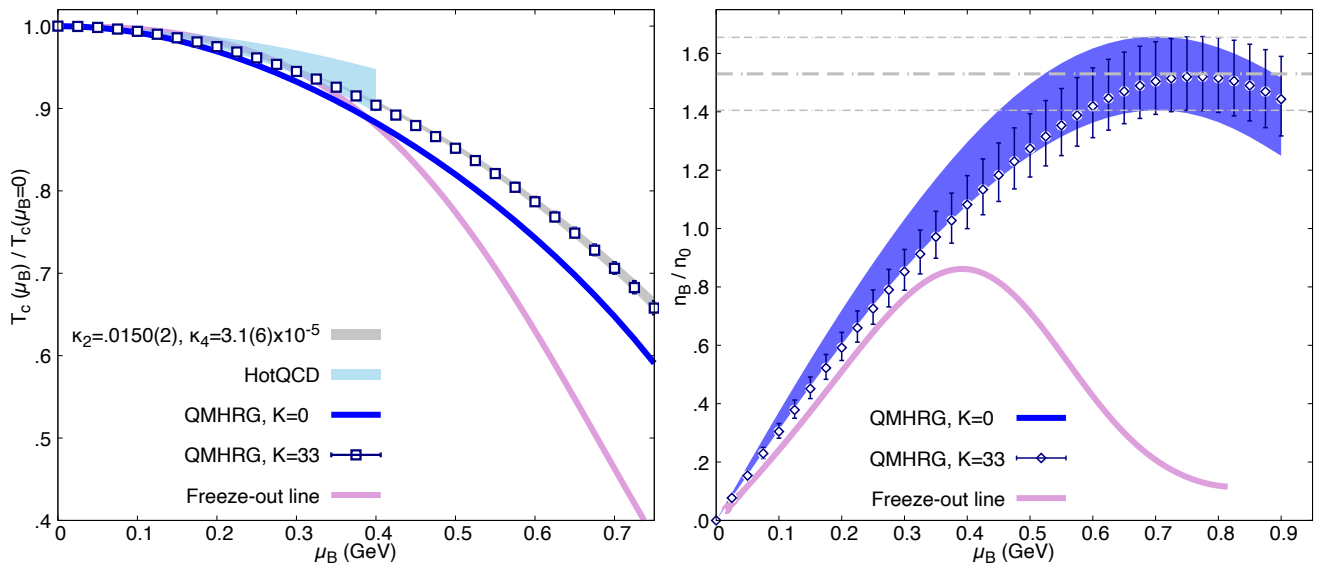


FIG. 3. (Left) The pseudo-critical line calculated from QMHRG model is compared with the lattice QCD results from HotQCD collaboration (light blue) from Ref. [61]. The ideal gas ($K = 0$) results are shown as a line and results including the mean-field repulsion ($K = 33$) are shown as open symbols. These are compared with the freeze-out line (magenta) using the parametrization in Ref. [62]. The gray line represents the fit performed by us for obtaining the pseudo-critical line, see text for details. (Right) The net-baryon density in units of $n_0 = 0.16 \text{ fm}^{-3}$ is shown as function of μ_B along the pseudo-critical line. We also show the variation of the net-baryon density along the freeze-out line. The color scheme is the same as in the left panel.

B. Curvature of the crossover line in the repulsive mean-field QMHRG model

As discussed in the previous subsection, the temperature at which the observable Δ_R^l falls to half its zero-temperature value, is used as an estimate of the pseudo-critical temperature T_c [27] for each value of μ_B . The extracted pseudo-critical temperature as a function of μ_B , $T_c(\mu_B)$ is shown as a function of μ_B in the left panel of Fig. 3 using QMHRG model for $K = 0$ and $K = 33 \text{ GeV}^{-2}$. The uncertainty in the value of Δ_R^l results in an uncertainty in the value of the crossover temperature, which, however, is quite small, about the size of the symbols in Fig. 3 or even smaller. In the same figure, the vertical axis is scaled by the estimated pseudo-critical temperatures at zero baryon density, which are $T_c(\mu_B = 0) = 161.2(1.7) \text{ MeV}$ for the ideal case [27], and $T_c(\mu_B = 0) = 161.5(1.6) \text{ MeV}$ for the repulsive QMHRG model with the mean-field coefficient $K = 33 \text{ GeV}^{-2}$, respectively. Our analysis is restricted to $\mu_B \leq 750 \text{ MeV}$ for reasons explained below. As one can see from the figure, the effects of repulsive baryon interactions start to have impact in the value of T_c for $\mu_B > 300 \text{ MeV}$ pushing the chiral crossover temperature toward larger values, and leading to a better agreement with the lattice QCD results on the curvature of the pseudo-critical line. On the other hand for $\mu_B < 300 \text{ MeV}$ the effects of the repulsive mean-fields are small, and good agreement for the curvature of the pseudo-critical line is obtained using QMHRG model with or without the repulsive mean-fields included.

In Fig. 3 we also show the recent parametrization of the chemical freeze-out line in heavy ion collisions from Ref. [62]. The freeze-out line is normalized by the freeze-out temperature $T_f = 158 \text{ MeV}$ at $\mu_B = 0$ [62]. For $\mu_B < 300 \text{ MeV}$ the freeze-out line agrees well with the pseudo-critical line. However, we observe significant differences between the pseudo-critical line and the chemical freeze-out line for $\mu_B > 400 \text{ MeV}$, which become larger as the value of the baryon chemical potential increases. Namely, the chiral crossover temperature is always larger than the chemical freeze-out temperature. For $\mu_B = 400 \text{ MeV}$, the chiral crossover temperature is more than 8 MeV larger than the freeze-out temperature while at $\mu_B = 750 \text{ MeV}$ it is more than 20 MeV larger than the freeze-out temperature. Thus, the system produced in heavy ion collisions in the fixed target mode of the RHIC beam energy scan program, as well as in the heavy ion collisions in GSI is expected to undergo a significant non-equilibrium chemical evolution in the hadronic phase unlike the matter produced in heavy ion collisions at higher center-of-mass energies, like the heavy ion collisions at LHC and RHIC in the collider mode.

We next performed a fit to the obtained values of $T_c(\mu_B)$ with the following widely used ansatz,

$$\frac{T_c(\mu_B)}{T_c(0)} = 1 - \kappa_2 \left(\frac{\mu_B}{T_c(0)} \right)^2 - \kappa_4 \left(\frac{\mu_B}{T_c(0)} \right)^4. \quad (8)$$

It turns out that a good fit can be obtained by this ansatz for $\mu_B \leq 750$ MeV which results in the following μ_B values of the curvature coefficients, $\kappa_2 = 0.0150(2)$ and $\kappa_4 = 3.1(6) \times 10^{-5}$. The value of κ_2 is consistent within errors with the two most recent continuum estimates from lattice QCD studies with physical masses, $\kappa_2 = 0.012(4)$ [61] and $\kappa_2 = 0.0153(18)$ [63], as well as with the earlier lattice QCD estimates [64–66]. For the first time, we could estimate a non-trivial value of κ_4 which is distinctly different from zero given the estimated errors. Lattice QCD calculations report a κ_4 which is compatible with zero within errors [61, 63]. The above estimate for the leading curvature coefficient is somewhat smaller than the one obtained from the relativistic nuclear mean-field model calculation, while κ_4 has the opposite sign [67]. Allowing for a non-zero value of κ_6 does not improve the quality of the fit, and only leads to much larger errors in κ_2 and κ_4 . Therefore, it is fair to say that within our accuracy, κ_6 is consistent with zero.

C. Net-baryon, energy density and particle composition along the pseudo-critical line

The right panel of Fig. 3 shows the estimated values of net-baryon density normalized by the nuclear saturation density n_0 as function of μ_B along the pseudo-critical line in $T - \mu_B$ plane. The baryon density increases monotonically with μ_B as expected, but for sufficiently large μ_B it reaches a maximum and then decreases with a further increase in μ_B . This behaviour is clearly unphysical and therefore, the applicability of the HRG model is restricted for large values of μ_B . The maximum in n_B of $1.53(13)n_0$ is reached at $\mu_B = 700$ MeV when $K = 0$ and at $\mu_B = 750$ MeV for $K = 33 \text{ GeV}^{-2}$. Thus the inclusion of repulsive mean-field interaction in the QMHRG model calculation helps to extend the model to slightly larger values of μ_B . However, our QMHRG model with a single repulsive mean-field is too simplistic and is not valid for very large values of μ_B . The large value of n_B obtained at relatively small values of μ_B is due to the contribution from baryon resonances. Since the chiral crossover temperature decreases with increasing μ_B , the contribution from these states will eventually decrease and the large value of the net-baryon density near the crossover point should come from nucleons and possibly their attractive interactions. But the simple HRG model cannot describe this switchover. Thus for temperatures close to the chiral crossover temperatures, the QMHRG model is only applicable for $\mu_B < 750$ MeV.

The non-monotonic variation of n_B with μ_B is also observed in the Nambu-Jona-Lasinio model [68], where the mass-gap equation determines the phase transition line, resulting in a qualitatively similar trend. A similar maximum of the net-baryon density as a function of μ_B was earlier observed in an HRG-motivated study along the freeze-out boundary in Ref. [69], which was determined from the hadron yields at different collision energies.

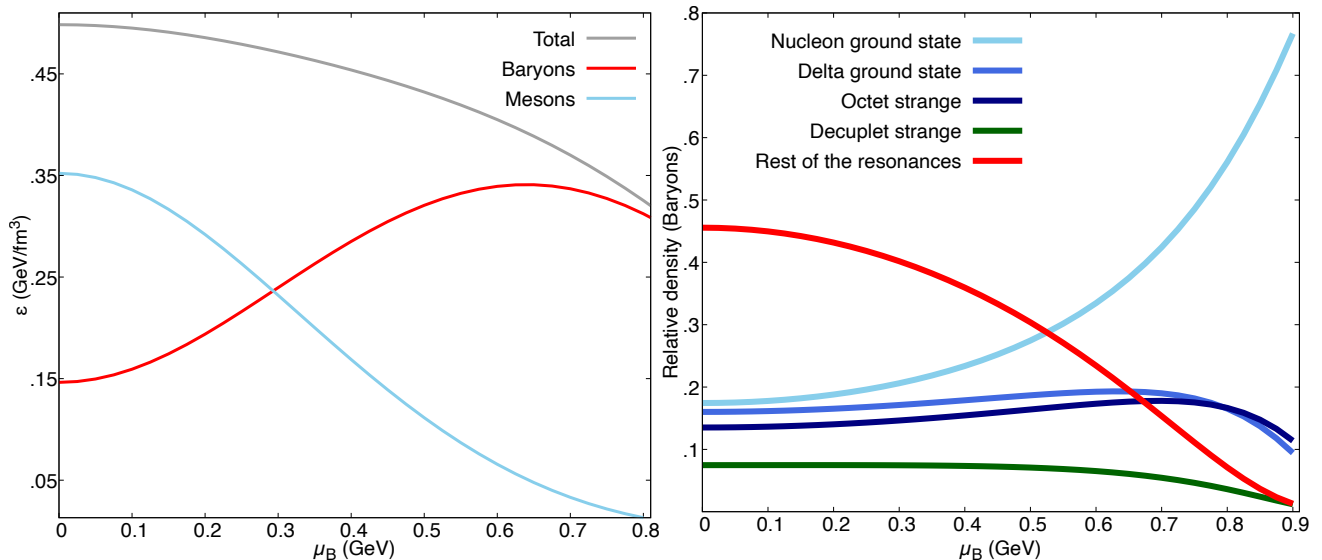


FIG. 4. (Left) Relative contributions to the energy density from mesons (blue) and baryons (red) along the pseudo-critical line compared to the total energy density (gray) calculated in the mean-field QMHRG model. (Right) The relative number densities of various baryon species shown along the pseudo-critical line.

It is interesting to study the variation of energy density along the pseudo-critical line, which is shown in the left panel of Fig. 4. As one can see that the energy density along the pseudo-critical line slightly decreases with increasing μ_B . The relative contribution to the energy density coming from baryon sector, increases till $\mu_B = 650$ MeV as the

baryon chemical potential increases, resulting in a shift from a meson-dominated to a baryon-dominated scenario, beyond $\mu_B = 350$ MeV. A comparable phenomenon can be observed in heavy-ion collisions, where a transition from meson to baryon dominance during freeze-out takes place at lower energies [70], where the net-baryon density is larger.

Furthermore, we would like to understand the relative abundances of different baryon species with increasing μ_B . In the right panel of Fig. 4 we have shown the relative contribution of different baryons and baryon-resonances to the net-baryon density as a function of μ_B along the pseudo-critical line. As the baryon chemical potential increases, the relative contribution of the nucleons also increases. The relative contributions of the lowest lying strange baryons and of the lowest Δ resonances do not change significantly with increasing μ_B , either. While the net contribution from higher lying resonances decreases with increasing μ_B , this contribution remains significant up to $\mu = 750$ MeV. Even for the largest value of $\mu_B = 750$ MeV, where our HRG model is applicable, nucleons contribute less than 50% to the total net-baryon density. Thus the contribution of the baryon resonances remains important even at large values of μ_B , and this contribution is responsible for the relatively large values on n_B . At the same time, the treatment of the repulsive interactions for baryon resonances is quite simplistic. In future, a more refined QMHRG mean-field model, which treats the repulsive interactions more differentially in the nucleon, strange baryon, and baryon resonance sectors will be needed to extend the reach of the QMHRG model.

D. Strangeness neutrality and the chiral pseudo-critical line

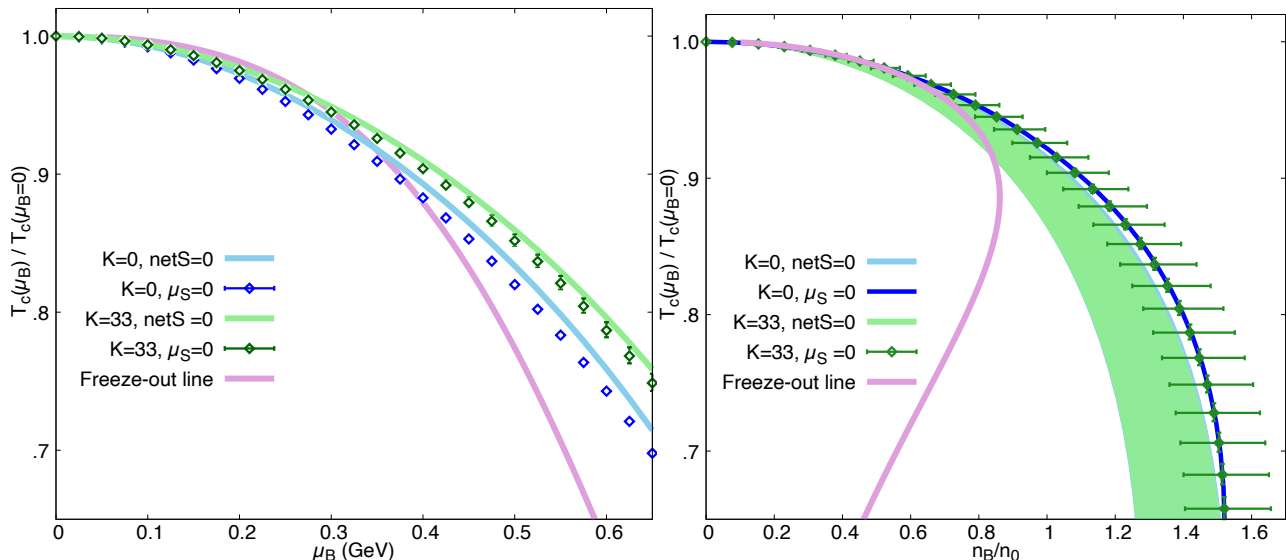


FIG. 5. The chiral crossover temperature at finite density μ_B normalized by its corresponding value at $\mu_B = 0$ is shown as function of μ_B (left) and as a function of n_B (right) for $\mu_S = 0$ and under strangeness neutrality condition, $n_S = 0$. Solid lines correspond to $n_S = 0$, while the data points represent the $\mu_S = 0$ condition. Ideal and repulsive mean-field QMHRG model results are shown in blue and green, respectively.

The system created in heavy ion collisions has zero net-strangeness, since the incoming nuclei do not contain strange particles. Therefore, it is important to estimate the pseudo-critical line for the conditions realized in heavy-ion experiments, namely for net-zero strangeness, $n_S = 0$. At non-zero values of μ_B , one needs to tune the strangeness chemical potential, μ_S to achieve zero net-strangeness. We performed this tuning for estimating the crossover temperature and the equation of state within our QMHRG model. The values of the μ_S needed to achieve strangeness neutrality are shown in Appendix C.

In Fig. 5 (left) we show the crossover temperature in the case of $n_S = 0$ as a function of the baryon chemical potential, while in Fig. 5 (right) we show the crossover temperature as a function of the net-baryon number. For a comparison, we also show our results for T_c for the unconstrained, $\mu_S = 0$ case in the same figure. We observe that imposing strangeness neutrality pushes the crossover temperature to a slightly larger values compared to the case of $\mu_S = 0$ discussed in the previous subsections, whether or not one includes the effect of the repulsive mean-field. The effect of imposing strangeness neutrality on the crossover temperature is considerably smaller than the effect of the repulsive interactions. Interestingly enough, the effects of the repulsive interactions are not visible on T_c when

plotted as a function of the net-baryon density. This can be seen from Fig. 5 (right). The clear difference between the pseudo-critical line and the freeze-out line is also apparent for the net-zero strangeness case, c.f. Fig. 5, especially when the results are shown in the $T - n_B$ plane.

The maximum net-baryon number density that can be reached within our model is slightly reduced compared to the unconstrained, $\mu_S = 0$ case to about $1.4n_0$ compared to $1.53n_0$ as obtained in the previous subsection. This is due to the fact that a positive non-zero value of μ_S required by the condition $n_S = 0$ reduces the contribution of strange baryons to the partition function.

V. SPEED OF SOUND ALONG THE ISENTROPIC LINES

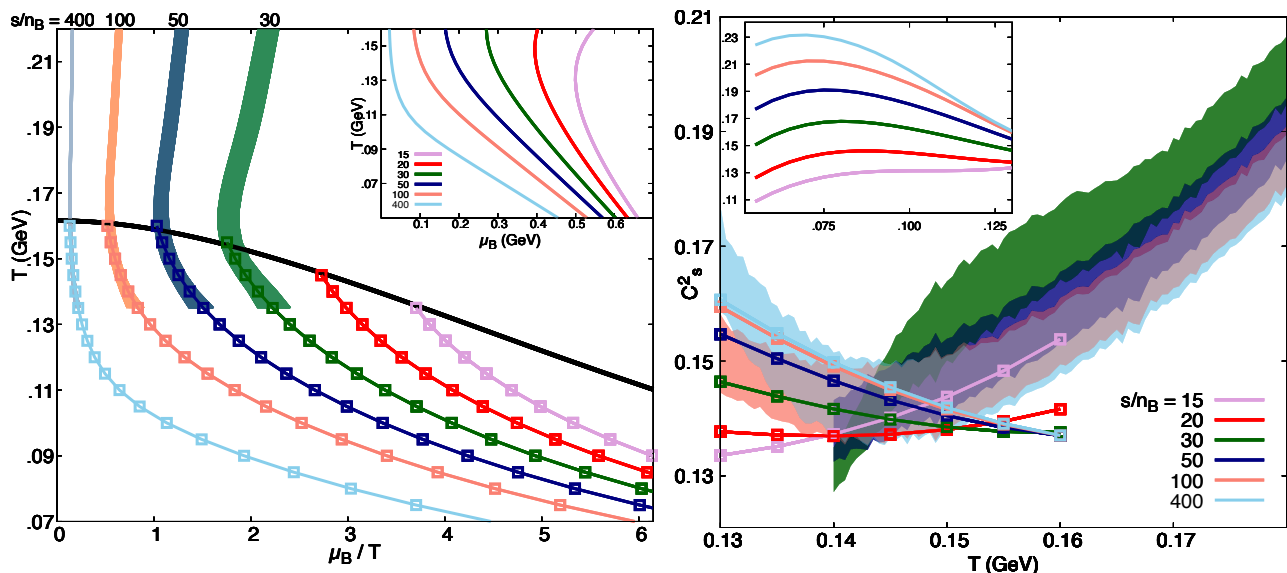


FIG. 6. (Left) The isentropes for $s/n_B = 15, 20, 30, 50, 100$ and 400 respectively are shown in the $T - \mu_B$ plane. (Right) The speed of sound as a function of the temperature is shown along these isentropes. The bands are the lattice QCD data from Ref. [29] and the points are the QMHRG model calculations with repulsive mean-field. The isentropes and the speed of sound in the low temperature region $60 < T < 150$ MeV are shown in the insets of the left and the right figures respectively. The black line represents the pseudo-critical line evaluated with our mean-field QMHRG.

In heavy-ion experiments, the chemical freeze-out surface is typically defined as a surface of constant entropy per baryon density, denoted as s/n_B [71]. Hence it is interesting to study the evolution of the QCD matter formed in heavy-ion collisions along the lines of constant s/n_B . The evolution of this matter is subject to several constraints, including strangeness neutrality ($n_S = 0$) and a fixed ratio of net electric charge (n_Q) to net-baryon number (n_B) density due to charge conservation. We study a particular case of strangeness-neutral condition with isospin symmetry which is realized when $n_Q/n_B = 0.5$ corresponding to a non-zero μ_B and μ_S but $\mu_Q = 0$. It has been shown that the differences in bulk thermodynamic observables that arise from deviations in n_Q/n_B from the isospin-symmetric value of 0.5 are minimal [29]. We have examined the isospin-symmetric scenario for a range of entropy per baryon density values, $s/n_B = 30, 50, 100$, and 400 . These values effectively cover the range of center of mass energies explored in the RHIC BES program in collider mode [29]. The left panel of Fig. 6 illustrates the isentropic trajectories for different values of s/n_B and compared to the lattice QCD results available up to $\mu_B/T = 2.5$ from Ref. [29]. We have also included the pseudo-critical line estimated by us in the same plot for comparison. Our estimates obtained within the mean-field repulsive QMHRG model show a good agreement with the lattice results at temperatures below the pseudo-critical temperatures. For completeness, we have also included the trajectories for $s/n_B = 15$ and $s/n_B = 20$ calculated within the repulsive QMHRG model. These trajectories are beyond the reach of lattice QCD calculations and hold significance for lower collision energies of the RHIC-BES program in the fixed target mode [72].

In the right panel of Fig. 6, we have shown the speed of sound calculated within the mean-field repulsive QMHRG

model calculated along these constant s/n_B trajectories. The speed of sound is defined as [29],

$$c_s^2 = \left(\frac{\partial P}{\partial \epsilon} \right)_{s/n_B, n_S, n_B/n_Q} = \frac{(\partial P / \partial T)_{s/n_B, n_S, n_B/n_Q}}{(\partial \epsilon / \partial T)_{s/n_B, n_S, n_B/n_Q}} \quad (9)$$

Here, all the derivatives are taken along the lines of constant $n_S = 0, n_B/n_Q = 0.5$ for different values of s/n_B . We show the speed of sound for our QMHRG model and compare it with the latest lattice QCD results from Ref. [29]. The c_s^2 calculated within the mean-field QMHRG model decreases as the temperature is increased towards T_c for $s/n_B > 30$. The QMHRG results with repulsive mean field for c_s^2 are in agreement with the lattice QCD results for $T < 150$ MeV. Beyond this temperature, the lattice QCD results show an increasing trend with the temperature, which cannot be reproduced within a QMHRG model, even when the effect of the repulsive interactions are included. We also observe that in the temperature range $100 \text{ MeV} < T < 150 \text{ MeV}$ the speed of sound decreases with increasing temperature both in the lattice QCD calculations and in the QMHRG model. This leads to a minimum of the speed of sound in the range of temperatures between 140-150 MeV. From the inset of Fig. 6 (right) we also observe that the speed of sound has a maximum in the low temperature region for $s/n_B \geq 30$.

The behaviour of the speed of sound for $s/n_B = 20$ and $s/n_B = 15$, currently inaccessible through lattice QCD techniques, is somewhat different. From Fig. 6 (right) we observe that for $s/n_B = 20$ the speed of sound has a very shallow minimum around $T = 145$ MeV, while for $s/n_B = 15$ it is always monotonically increasing with increasing temperatures. This implies that the maximum in c_s^2 seen at low temperatures and small baryon densities disappears. Thus there is no softening of the equation of state near the chiral crossover transition at large values of baryon densities corresponding to $s/n_B < 15$.

VI. SUMMARY

In this paper, we have studied the QCD equation of state and the chiral crossover at non-zero net baryon density using the QMHRG model with repulsive mean-field interaction. We have shown that this model can describe the lattice results on the fluctuations of net baryon number up to the eighth order in the vicinity of the chiral crossover temperature if the parameter characterizing the strength of the mean-field repulsive interactions is properly chosen. This is contrary to the usual QMHRG which can describe the higher order net baryon number fluctuations only for considerably lower temperatures.

We extended our previous calculation of the chiral crossover temperature within the QMHRG model limited to the region of small baryon chemical potential [27] to much larger values of the baryon chemical potential. We showed that for $\mu_B > 400$ MeV there is a significant effect of the repulsive mean-field on the value of the chiral crossover temperature. We found that the μ_B -dependence of the chiral crossover temperature can be very well parametrized by the following form, $T_c(\mu_B)/T_c(0) = 1 - \kappa_2(\mu_B/T_c(0))^2 - \kappa_4(\mu_B/T_c(0))^4$ with $\kappa_2 = 0.0150(2)$ and $\kappa_4 = 3.1(6) \cdot 10^{-5}$. The value of the leading curvature coefficient, κ_2 agrees well with the lattice QCD results within errors. The smallness of κ_4 is consistent with the upper bounds from lattice QCD, but for the first time we found that the corresponding value is significantly different from zero.

To realize the relevance of this study in the context of heavy-ion collision experiments, we have estimated the chiral crossover line imposing the strangeness-neutrality condition. The separation between the freeze-out curve and the pseudo-critical line increases toward high density, which implies a longer-lived interacting hadronic phase at lower collision energies. Furthermore, we have used the repulsive mean-field QMHRG model to calculate the speed of sound along various isentropic (constant s/n_B) lines pertinent to the heavy-ion collision experiments, constrained by the strangeness-neutrality and n_Q/n_B ratio. In the hadron phase, there is good agreement between our calculation and the latest available data in lattice QCD. We have also predicted the isentropic trajectory and the speed of sound within this repulsive mean-field model for $s/n_B = 15$, where no lattice QCD data is available. We see that starting from this value of s/n_B the previously seen characteristic softening of the QCD equation of state near the chiral crossover regions disappears.

We pointed out that the QMHRG model with a single repulsive mean field for all baryons only works for $\mu_B < 750$ MeV. For larger values of the baryon chemical potential, a more refined mean field approach is needed, which has different mean-fields for different baryon species.

ACKNOWLEDGMENTS

P.P. is supported by the U.S. Department of Energy, Office of Science, through Contract No. DE-SC0012704. S.S. gratefully acknowledges support from the Department of Science and Technology, Government of India through a

Ramanujan Fellowship. D.B. gratefully acknowledges Jishnu Goswami for helping with the lattice data from the HotQCD collaboration. Additionally, D.B would like to extend thanks to Aman Abhishek, Hiranmaya Mishra and Nachiketa Sarkar for useful discussions.

Appendix A: Calculation of baryon number fluctuations within mean-field HRG

The fluctuations of baryon charges can be derived from the pressure as the following [55],

$$\chi_B^n = \frac{\partial^n [P(\mu_B/T)/T^4]}{\partial(\mu_B/T)^n} \quad (\text{A1})$$

In the mean-field formalism, the respective number densities for baryons and anti-baryons in Boltzmann approximation are written as [46],

$$n_b = \sum_{i=B} \int g_i \frac{d^3p}{(2\pi)^3} e^{-\beta(E_i - \mu_B + Kn_b)} \quad \text{and} \quad n_{\bar{b}} = \sum_{i=\bar{B}} \int g_i \frac{d^3p}{(2\pi)^3} e^{-\beta(E_i + \mu_B + Kn_{\bar{b}})} \quad (\text{A2})$$

Here, β is the inverse of temperature. The above equations are transcendental equations and one can evaluate the fluctuations of the net baryon number by taking the derivative with μ_B/T .

$$\frac{\partial n_b}{\partial(\beta\mu_B)} = \sum_{i=B} g_i \int \frac{d^3p}{(2\pi)^3} e^{-\beta(E_i - \mu_B + Kn_b)} \left[1 - \beta K \frac{\partial n_b}{\partial(\beta\mu_B)} \right] = \sum_{i=B} n_i \left[1 - \beta K \frac{\partial n_b}{\partial(\beta\mu_B)} \right] \quad (\text{A3})$$

By re-arranging the above equation, one can write the first derivative as,

$$n'_b = \frac{\partial n_b}{\partial(\beta\mu_B)} = \frac{\sum_{i=B} n_i}{[1 + \beta K \sum_{i=B} n_i]} = \frac{n_b}{[1 + \beta K n_b]} \quad (\text{A4})$$

Similarly for the anti-baryon sector,

$$n'_{\bar{b}} = \frac{\partial n_{\bar{b}}}{\partial(\beta\mu_B)} = \frac{-\sum_{i=\bar{B}} n_i}{[1 + \beta K \sum_{i=\bar{B}} n_i]} = \frac{-n_{\bar{b}}}{[1 + \beta K n_{\bar{b}}]} \quad (\text{A5})$$

In the mean-field formalism, the total pressure in the baryon sector is written as a sum of the partial pressure of the (anti-)baryons [46],

$$P = T(n_b + n_{\bar{b}}) + \frac{K}{2}(n_b^2 + n_{\bar{b}}^2) \quad \text{and} \quad \frac{P}{T^4} = \beta^3(n_b + n_{\bar{b}}) + \beta^4 \frac{K}{2}(n_b^2 + n_{\bar{b}}^2)$$

Taking one order derivative w.r.t $\beta\mu_B$ we get

$$\begin{aligned} \chi_B^1 &= \beta^3(n'_b + n'_{\bar{b}}) + \beta^4 K(n_b n'_b + n_{\bar{b}} n'_{\bar{b}}) = \beta^3 n'_b (1 + \beta K n_b) + \beta^3 n'_{\bar{b}} (1 + \beta K n_{\bar{b}}) \\ &= \beta^3 (n_b - n_{\bar{b}}) \end{aligned} \quad (\text{A6})$$

The above equation ensures that the net baryon number is given by the difference of the number of baryons and the number of anti-baryons, and vanishes for $\mu_B = 0$.

Using the above expressions, it is easy to extend the calculations to higher-order derivatives w.r.t μ_B/T . For completeness here we are enlisting all the derivatives up to the 8th order.

$$\begin{aligned} \chi_B^1 &= \beta^3 [n_b - n_{\bar{b}}] \\ \chi_B^2 &= \beta^3 \left[\frac{n_b}{(1 + \beta K n_b)} + \frac{n_{\bar{b}}}{(1 + \beta K n_{\bar{b}})} \right] \\ \chi_B^3 &= \beta^3 \left[\frac{n_b}{(1 + \beta K n_b)^3} - \frac{n_{\bar{b}}}{(1 + \beta K n_{\bar{b}})^3} \right] \end{aligned} \quad (\text{A7})$$

$$\begin{aligned}
\chi_B^4 &= \beta^3 \left[\frac{n_b(1-2\beta Kn_b)}{(1+\beta Kn_b)^5} + \frac{n_{\bar{b}}(1-2\beta Kn_{\bar{b}})}{(1+\beta Kn_{\bar{b}})^5} \right] \\
\chi_B^5 &= \beta^3 \left[\frac{n_b(1-8\beta Kn_b+6[\beta Kn_b]^2)}{(1+\beta Kn_b)^7} - \frac{n_{\bar{b}}(1-8\beta Kn_{\bar{b}}+6[\beta Kn_{\bar{b}}]^2)}{(1+\beta Kn_{\bar{b}})^7} \right] \\
\chi_B^6 &= \beta^3 \left[\frac{n_b(1-22\beta Kn_b+58[\beta Kn_b]^2-24[\beta Kn_b]^3)}{(1+\beta Kn_b)^9} + \frac{n_{\bar{b}}(1-22\beta Kn_{\bar{b}}+58[\beta Kn_{\bar{b}}]^2-24[\beta Kn_{\bar{b}}]^3)}{(1+\beta Kn_{\bar{b}})^9} \right] \\
\chi_B^7 &= \beta^3 \left[\frac{n_b(1-52\beta Kn_b+328[\beta Kn_b]^2-444[\beta Kn_b]^3+120[\beta Kn_b]^4)}{(1+\beta Kn_b)^{11}} \right] - \\
&\quad \beta^3 \left[\frac{n_{\bar{b}}(1-52\beta Kn_{\bar{b}}+328[\beta Kn_{\bar{b}}]^2-444[\beta Kn_{\bar{b}}]^3+120[\beta Kn_{\bar{b}}]^4)}{(1+\beta Kn_{\bar{b}})^{11}} \right] \\
\chi_B^8 &= \beta^3 \left[\frac{n_b(1-114\beta Kn_b+1452[\beta Kn_b]^2-4400[\beta Kn_b]^3+3708[\beta Kn_b]^4-720[\beta Kn_b]^5)}{(1+\beta Kn_b)^{13}} \right] + \\
&\quad \beta^3 \left[\frac{n_{\bar{b}}(1-114\beta Kn_{\bar{b}}+1452[\beta Kn_{\bar{b}}]^2-4400[\beta Kn_{\bar{b}}]^3+3708[\beta Kn_{\bar{b}}]^4-720[\beta Kn_{\bar{b}}]^5)}{(1+\beta Kn_{\bar{b}})^{13}} \right]
\end{aligned}$$

It is obvious from the above equations that the odd fluctuations of net baryon number vanish for $\mu_B = 0$.

Using the above expression we calculated the fluctuations of the net baryon density up to the 8th order at $\mu_B = 0$ and compared them to the available lattice results for different values of the parameter K . The value $K = 33 \text{ GeV}^{-2}$ leads to a good agreement with the lattice QCD results as one sees from Fig. 7. Here it is assumed that all baryons and baryon resonances contribute to the mean field. If we assume that only ground-state baryons contribute to the mean field then we do not get such a good agreement with the lattice QCD results for the same value of K . However, using a larger value of K , namely $K = 100 \text{ GeV}^{-2}$ a reasonably good agreement with the lattice QCD results can be obtained, cf. Fig. 7.

Appendix B: Calculation of the equation of state within the mean-field HRG model

The energy density is defined from the pressure as,

$$\epsilon = -P - \beta \left(\frac{\partial P}{\partial \beta} \right)_{\beta\mu}. \quad (\text{B1})$$

Taking the derivative of the number density with β we find,

$$\begin{aligned}
\left(\frac{\partial n_b}{\partial \beta} \right)_{\beta\mu} &= \sum_{i=B} g_i \int \frac{d^3p}{(2\pi)^3} e^{-\beta(E_i - \mu_B + Kn_b)} \times \left[-E_i - Kn_b - \beta K \left(\frac{\partial n_b}{\partial \beta} \right)_{\beta\mu} \right] \\
&= - \sum_{i=B} g_i \int \frac{d^3p}{(2\pi)^3} f_i^b E_i - Kn_b^2 - \beta Kn_b \left(\frac{\partial n_b}{\partial \beta} \right)_{\beta\mu}. \quad (\text{B2})
\end{aligned}$$

Rearranging the above equation we get,

$$\left(\frac{\partial n_b}{\partial \beta} \right)_{\beta\mu} = \frac{- \sum_{i=B} g_i \int \frac{d^3p}{(2\pi)^3} f_i^b E_i - Kn_b^2}{1 + \beta Kn_b}. \quad (\text{B3})$$

Similarly for the anti-baryon, we can write,

$$\left(\frac{\partial n_{\bar{b}}}{\partial \beta} \right)_{\beta\mu} = \frac{- \sum_{i=\bar{B}} g_i \int \frac{d^3p}{(2\pi)^3} f_i^{\bar{b}} E_i - Kn_{\bar{b}}^2}{1 + \beta Kn_{\bar{b}}}. \quad (\text{B4})$$

The derivative of the pressure is written as

$$\begin{aligned}
-\beta \left(\frac{\partial P}{\partial \beta} \right)_{\beta\mu} &= +\frac{1}{\beta}(n_b + n_{\bar{b}}) - \left(\frac{\partial n_b}{\partial \beta} \right)_{\beta\mu} (1 + \beta Kn_b) - \left(\frac{\partial n_{\bar{b}}}{\partial \beta} \right)_{\beta\mu} (1 + \beta Kn_{\bar{b}}) \\
&= +\frac{1}{\beta}(n_b + n_{\bar{b}}) + \sum_{i=B} g_i \int \frac{d^3p}{(2\pi)^3} f_i^b E_i + Kn_b^2 + \sum_{i=\bar{B}} g_i \int \frac{d^3p}{(2\pi)^3} f_i^{\bar{b}} E_i + Kn_{\bar{b}}^2. \quad (\text{B5})
\end{aligned}$$

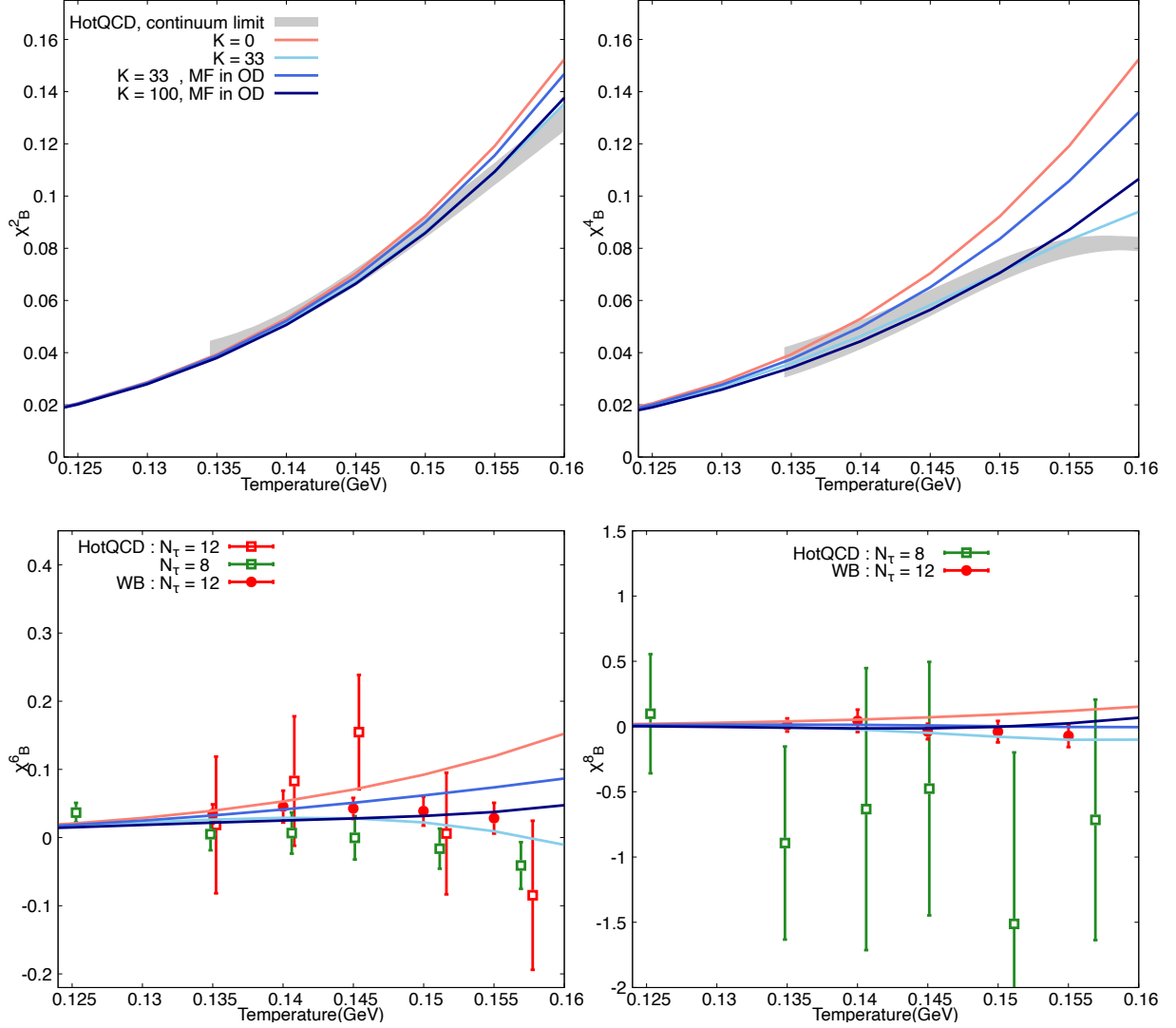


FIG. 7. Top row: The second (left) and fourth (right) order, bottom row: sixth (left) and eighth (right) order baryon number fluctuations are shown as a function of temperature and $\mu_B = 0$. The $K = 0$ results represent the ideal QMHRG model, whereas the $K = 33$ data are calculated with mean-field repulsive interactions among all the baryons with a mean-field coefficient of $K = 33 \text{ GeV}^{-2}$. Similarly, MF in OD represents the case where we have included repulsive mean-field interaction only among the baryons in octet and decuplet. Lattice QCD results for $N_\tau = 8$ and $N_\tau = 12$ are shown in red and green colors respectively where the square and circles correspond to data from the HotQCD [55] and Wuppertal-Budapest (WB) [2] collaborations.

Putting the derivative terms altogether in Eq.B1 one can derive the final expression for the energy density,

$$\begin{aligned}
 \epsilon &= -\frac{1}{\beta}(n_b + n_{\bar{b}}) - \frac{K}{2}(n_b^2 + n_{\bar{b}}^2) + \frac{1}{\beta}(n_b + n_{\bar{b}}) + \sum_{i=B} g_i \int \frac{d^3p}{(2\pi)^3} f_i^b E_i + \sum_{i=\bar{B}} g_i \int \frac{d^3p}{(2\pi)^3} f_i^{\bar{b}} E_i + K(n_b^2 + n_{\bar{b}}^2) \\
 &= \sum_{i=B} g_i \int \frac{d^3p}{(2\pi)^3} f_i^b E_i + \sum_{i=\bar{B}} g_i \int \frac{d^3p}{(2\pi)^3} f_i^{\bar{b}} E_i + \frac{K}{2}(n_b^2 + n_{\bar{b}}^2)
 \end{aligned} \tag{B6}$$

In the ideal limit of $K = 0$ the above formula reduces to the ideal HRG expression for energy density. In Fig. 8 we show the pressure and energy density in units of T^4 in QMHRG and compare them with the lattice QCD results from Ref. [1]. The results for both the ideal case and repulsive mean-field case with $K = 33 \text{ GeV}^{-2}$ at $\mu_B/T = 0, 1, \text{ and } 2$ are displayed. For all baryon chemical potentials, the QMHRG estimations align well with lattice results up to 150 MeV. At high μ_B/T , the effect of repulsive mean-field is more pronounced due to the increased thermal abundance of baryons at high density, cf. Fig. 8.

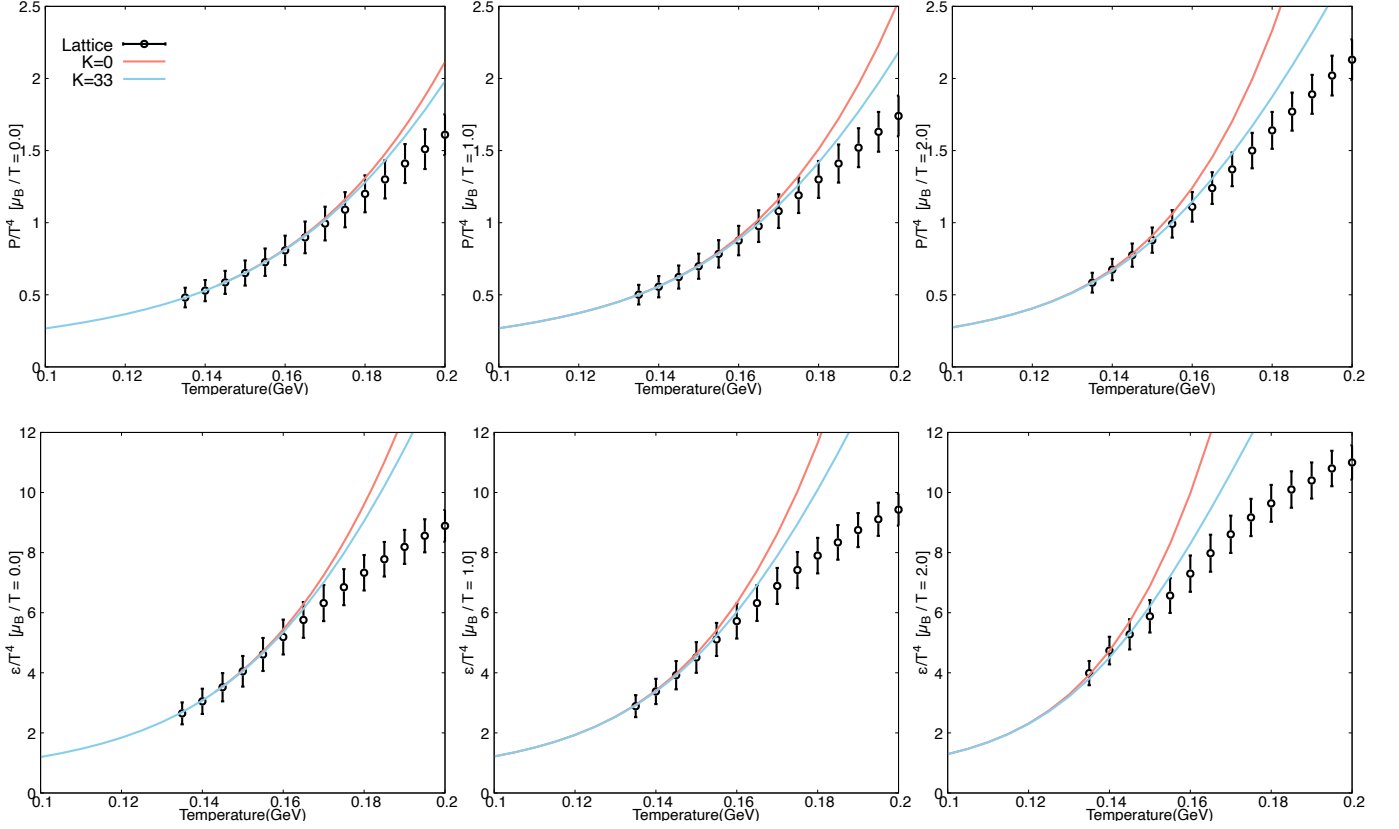


FIG. 8. The pressure P/T^4 (upper row) and energy density ϵ/T^4 (lower row) normalized by T^4 calculated for ideal (red) and repulsive mean-field (blue) QMHRG model. Lattice results (black points) are from Ref. [1]. The results are displayed for $\mu_B/T = 0, 1$, and 2 , in the left, middle and right panels respectively.

Appendix C: Strangeness chemical potential for strange neutrality case

In Fig. 9 (left) we show the temperature normalized baryon and strangeness chemical potential along the chiral crossover line for $n_S = 0$. We see that the effect of the repulsive mean-field is visible for the baryon chemical potential, but is very small for the strangeness chemical potential. In Fig. 9 (right) we show the ratio μ_S/μ_B along the crossover line. We see that the repulsive mean-field significantly reduces this ratio compared to the ideal case.

-
- [1] A. Bazavov, et al., The QCD Equation of State to $\mathcal{O}(\mu_B^6)$ from Lattice QCD, Phys. Rev. D 95 (5) (2017) 054504. [arXiv:1701.04325](https://arxiv.org/abs/1701.04325), [doi:10.1103/PhysRevD.95.054504](https://doi.org/10.1103/PhysRevD.95.054504).
- [2] S. Borsanyi, Z. Fodor, J. N. Guenther, S. K. Katz, K. K. Szabo, A. Pasztor, I. Portillo, C. Ratti, Higher order fluctuations and correlations of conserved charges from lattice QCD, JHEP 10 (2018) 205. [arXiv:1805.04445](https://arxiv.org/abs/1805.04445), [doi:10.1007/JHEP10\(2018\)205](https://doi.org/10.1007/JHEP10(2018)205).
- [3] M. D'Elia, G. Gagliardi, F. Sanfilippo, Higher order quark number fluctuations via imaginary chemical potentials in $N_f = 2 + 1$ QCD, Phys. Rev. D 95 (9) (2017) 094503. [arXiv:1611.08285](https://arxiv.org/abs/1611.08285), [doi:10.1103/PhysRevD.95.094503](https://doi.org/10.1103/PhysRevD.95.094503).
- [4] D. Bollweg, J. Goswami, O. Kaczmarek, F. Karsch, S. Mukherjee, P. Petreczky, C. Schmidt, P. Scior, Taylor expansions and Padé approximants for cumulants of conserved charge fluctuations at nonvanishing chemical potentials, Phys. Rev. D 105 (7) (2022) 074511. [arXiv:2202.09184](https://arxiv.org/abs/2202.09184), [doi:10.1103/PhysRevD.105.074511](https://doi.org/10.1103/PhysRevD.105.074511).
- [5] S. Borsányi, Z. Fodor, J. N. Guenther, R. Kara, S. D. Katz, P. Parotto, A. Pásztor, C. Ratti, K. K. Szabó, Lattice QCD equation of state at finite chemical potential from an alternative expansion scheme, Phys. Rev. Lett. 126 (23) (2021) 232001. [arXiv:2102.06660](https://arxiv.org/abs/2102.06660), [doi:10.1103/PhysRevLett.126.232001](https://doi.org/10.1103/PhysRevLett.126.232001).
- [6] R. Dashen, S.-K. Ma, H. J. Bernstein, S Matrix formulation of statistical mechanics, Phys. Rev. 187 (1969) 345–370. [doi:10.1103/PhysRev.187.345](https://doi.org/10.1103/PhysRev.187.345).

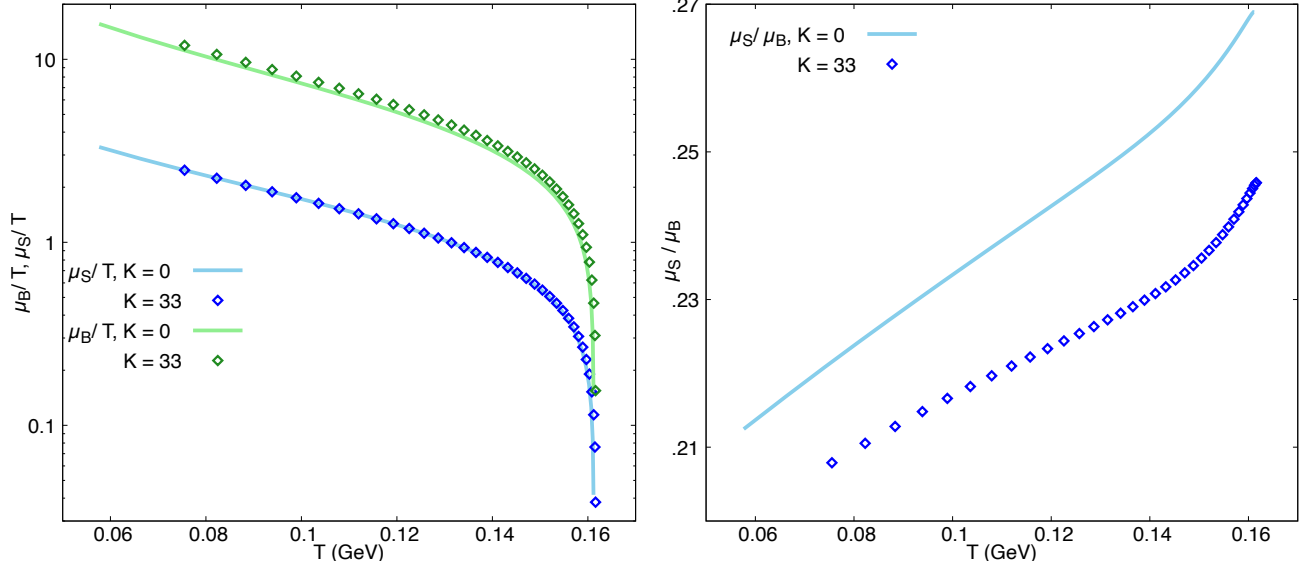


FIG. 9. The chemical potentials μ_B/T and μ_S/T (left) and the ratio μ_B/μ_S (right) are shown for different temperatures along the pseudo-critical line. The $K = 0$ denotes ideal QMHRG model results, whereas $K = 33$ represents the case where we have included repulsive interaction among all baryons with a mean-field coefficient of $K = 33 \text{ GeV}^{-2}$.

- [7] R. Venugopalan, M. Prakash, Thermal properties of interacting hadrons, Nucl. Phys. A 546 (1992) 718–760. doi: 10.1016/0375-9474(92)90005-5.
- [8] F. Karsch, K. Redlich, A. Tawfik, Hadron resonance mass spectrum and lattice QCD thermodynamics, Eur. Phys. J. C 29 (2003) 549–556. arXiv:hep-ph/0303108, doi:10.1140/epjc/s2003-01228-y.
- [9] F. Karsch, K. Redlich, A. Tawfik, Thermodynamics at nonzero baryon number density: A Comparison of lattice and hadron resonance gas model calculations, Phys. Lett. B 571 (2003) 67–74. arXiv:hep-ph/0306208, doi:10.1016/j.physletb.2003.08.001.
- [10] S. Ejiri, F. Karsch, K. Redlich, Hadronic fluctuations at the QCD phase transition, Phys. Lett. B 633 (2006) 275–282. arXiv:hep-ph/0509051, doi:10.1016/j.physletb.2005.11.083.
- [11] P. Huovinen, P. Petreczky, QCD Equation of State and Hadron Resonance Gas, Nucl. Phys. A 837 (2010) 26–53. arXiv:0912.2541, doi:10.1016/j.nuclphysa.2010.02.015.
- [12] S. Borsanyi, Z. Fodor, C. Hoelbling, S. D. Katz, S. Krieg, C. Ratti, K. K. Szabo, Is there still any T_c mystery in lattice QCD? Results with physical masses in the continuum limit III, JHEP 09 (2010) 073. arXiv:1005.3508, doi: 10.1007/JHEP09(2010)073.
- [13] A. Bazavov, et al., Fluctuations and Correlations of net baryon number, electric charge, and strangeness: A comparison of lattice QCD results with the hadron resonance gas model, Phys. Rev. D 86 (2012) 034509. arXiv:1203.0784, doi: 10.1103/PhysRevD.86.034509.
- [14] S. Borsanyi, Z. Fodor, C. Hoelbling, S. D. Katz, S. Krieg, K. K. Szabo, Full result for the QCD equation of state with 2+1 flavors, Phys. Lett. B 730 (2014) 99–104. arXiv:1309.5258, doi:10.1016/j.physletb.2014.01.007.
- [15] A. Bazavov, et al., Equation of state in (2+1)-flavor QCD, Phys. Rev. D 90 (2014) 094503. arXiv:1407.6387, doi: 10.1103/PhysRevD.90.094503.
- [16] A. Bazavov, P. Petreczky, J. H. Weber, Equation of State in 2+1 Flavor QCD at High Temperatures, Phys. Rev. D 97 (1) (2018) 014510. arXiv:1710.05024, doi:10.1103/PhysRevD.97.014510.
- [17] R. Bellwied, S. Borsanyi, Z. Fodor, S. D. Katz, A. Pasztor, C. Ratti, K. K. Szabo, Fluctuations and correlations in high temperature QCD, Phys. Rev. D 92 (11) (2015) 114505. arXiv:1507.04627, doi:10.1103/PhysRevD.92.114505.
- [18] D. Bollweg, J. Goswami, O. Kaczmarek, F. Karsch, S. Mukherjee, P. Petreczky, C. Schmidt, P. Scior, Second order cumulants of conserved charge fluctuations revisited: Vanishing chemical potentials, Phys. Rev. D 104 (7) (2021) 074512. arXiv:2107.10011, doi:10.1103/PhysRevD.104.074512.
- [19] A. Bazavov, et al., Additional Strange Hadrons from QCD Thermodynamics and Strangeness Freezeout in Heavy Ion Collisions, Phys. Rev. Lett. 113 (7) (2014) 072001. arXiv:1404.6511, doi:10.1103/PhysRevLett.113.072001.
- [20] A. Bazavov, et al., The melting and abundance of open charm hadrons, Phys. Lett. B 737 (2014) 210–215. arXiv:1404.4043, doi:10.1016/j.physletb.2014.08.034.
- [21] R. Bellwied, S. Borsanyi, Z. Fodor, J. N. Guenther, J. Noronha-Hostler, P. Parotto, A. Pasztor, C. Ratti, J. M. Stafford, Off-diagonal correlators of conserved charges from lattice QCD and how to relate them to experiment, Phys. Rev. D 101 (3) (2020) 034506. arXiv:1910.14592, doi:10.1103/PhysRevD.101.034506.

- [22] C. Fernández-Ramírez, P. M. Lo, P. Petreczky, Thermodynamics of the strange baryon system from a coupled-channels analysis and missing states, *Phys. Rev. C* 98 (4) (2018) 044910. [arXiv:1806.02177](#), [doi:10.1103/PhysRevC.98.044910](#).
- [23] P. Gerber, H. Leutwyler, Hadrons Below the Chiral Phase Transition, *Nucl. Phys. B* 321 (1989) 387–429. [doi:10.1016/0550-3213\(89\)90349-0](#).
- [24] D. Toublan, J. B. Kogut, The QCD phase diagram at nonzero baryon, isospin and strangeness chemical potentials: Results from a hadron resonance gas model, *Phys. Lett. B* 605 (2005) 129–136. [arXiv:hep-ph/0409310](#), [doi:10.1016/j.physletb.2004.11.018](#).
- [25] J. Jankowski, D. Blaschke, M. Spalinski, Chiral condensate in hadronic matter, *Phys. Rev. D* 87 (10) (2013) 105018. [arXiv:1212.5521](#), [doi:10.1103/PhysRevD.87.105018](#).
- [26] J. O. Andersen, Q. Yu, H. Zhou, Thermodynamics and quark condensates of three-flavor QCD at low temperature, *Phys. Rev. D* 107 (1) (2023) 014010. [arXiv:2205.03072](#), [doi:10.1103/PhysRevD.107.014010](#).
- [27] D. Biswas, P. Petreczky, S. Sharma, Chiral condensate from a hadron resonance gas model, *Phys. Rev. C* 106 (4) (2022) 045203. [arXiv:2206.04579](#), [doi:10.1103/PhysRevC.106.045203](#).
- [28] W.-j. Fu, J. M. Pawłowski, F. Rennecke, QCD phase structure at finite temperature and density, *Phys. Rev. D* 101 (5) (2020) 054032. [arXiv:1909.02991](#), [doi:10.1103/PhysRevD.101.054032](#).
- [29] D. Bollweg, D. A. Clarke, J. Goswami, O. Kaczmarek, F. Karsch, S. Mukherjee, P. Petreczky, C. Schmidt, S. Sharma, Equation of state and speed of sound of (2+1)-flavor QCD in strangeness-neutral matter at nonvanishing net baryon-number density, *Phys. Rev. D* 108 (1) (2023) 014510. [arXiv:2212.09043](#), [doi:10.1103/PhysRevD.108.014510](#).
- [30] D. H. Rischke, M. I. Gorenstein, H. Stoecker, W. Greiner, Excluded volume effect for the nuclear matter equation of state, *Z. Phys. C* 51 (1991) 485–490. [doi:10.1007/BF01548574](#).
- [31] J. Cleymans, M. I. Gorenstein, J. Stalnacke, E. Suhonen, Excluded volume effect and the quark - hadron phase transition, *Phys. Scripta* 48 (1993) 277–280. [doi:10.1088/0031-8949/48/3/004](#).
- [32] G. D. Yen, M. I. Gorenstein, W. Greiner, S.-N. Yang, Excluded volume hadron gas model for particle number ratios in A+A collisions, *Phys. Rev. C* 56 (1997) 2210–2218. [arXiv:nucl-th/9711062](#), [doi:10.1103/PhysRevC.56.2210](#).
- [33] S. K. Tiwari, P. K. Srivastava, C. P. Singh, Description of Hot and Dense Hadron Gas Properties in a New Excluded-Volume model, *Phys. Rev. C* 85 (2012) 014908. [arXiv:1111.2406](#), [doi:10.1103/PhysRevC.85.014908](#).
- [34] A. Bhattacharyya, S. Das, S. K. Ghosh, R. Ray, S. Samanta, Fluctuations and correlations of conserved charges in an excluded volume hadron resonance gas model, *Phys. Rev. C* 90 (3) (2014) 034909. [arXiv:1310.2793](#), [doi:10.1103/PhysRevC.90.034909](#).
- [35] M. Albricht, J. Kapusta, C. Young, Matching Excluded Volume Hadron Resonance Gas Models and Perturbative QCD to Lattice Calculations, *Phys. Rev. C* 90 (2) (2014) 024915. [arXiv:1404.7540](#), [doi:10.1103/PhysRevC.90.024915](#).
- [36] G. P. Kadam, H. Mishra, Dissipative properties of hot and dense hadronic matter in an excluded-volume hadron resonance gas model, *Phys. Rev. C* 92 (3) (2015) 035203. [arXiv:1506.04613](#), [doi:10.1103/PhysRevC.92.035203](#).
- [37] G. P. Kadam, Curing the acausal behavior of the sound velocity in an excluded volume hadron resonance gas model (2015). [arXiv:1510.04371](#).
- [38] V. Vovchenko, M. I. Gorenstein, H. Stoecker, van der Waals Interactions in Hadron Resonance Gas: From Nuclear Matter to Lattice QCD, *Phys. Rev. Lett.* 118 (18) (2017) 182301. [arXiv:1609.03975](#), [doi:10.1103/PhysRevLett.118.182301](#).
- [39] V. Vovchenko, A. Motornenko, P. Alba, M. I. Gorenstein, L. M. Satarov, H. Stoecker, Multicomponent van der Waals equation of state: Applications in nuclear and hadronic physics, *Phys. Rev. C* 96 (4) (2017) 045202. [arXiv:1707.09215](#), [doi:10.1103/PhysRevC.96.045202](#).
- [40] S. Samanta, B. Mohanty, Criticality in a Hadron Resonance Gas model with the van der Waals interaction, *Phys. Rev. C* 97 (1) (2018) 015201. [arXiv:1709.04446](#), [doi:10.1103/PhysRevC.97.015201](#).
- [41] N. Sarkar, P. Ghosh, van der Waals hadron resonance gas and QCD phase diagram, *Phys. Rev. C* 98 (1) (2018) 014907. [arXiv:1807.02948](#), [doi:10.1103/PhysRevC.98.014907](#).
- [42] V. Vovchenko, Hadron resonance gas with van der Waals interactions, *Int. J. Mod. Phys. E* 29 (05) (2020) 2040002. [arXiv:2004.06331](#), [doi:10.1142/S0218301320400029](#).
- [43] K. A. Olive, The Thermodynamics of the Quark - Hadron Phase Transition in the Early Universe, *Nucl. Phys. B* 190 (1981) 483–503. [doi:10.1016/0550-3213\(81\)90444-2](#).
- [44] K. A. Olive, THE QUARK - HADRON TRANSITION IN SYSTEMS WITH NET BARYON NUMBER, *Nucl. Phys. B* 198 (1982) 461–473. [doi:10.1016/0550-3213\(82\)90335-2](#).
- [45] J. I. Kapusta, K. A. Olive, Thermodynamics of Hadrons: Delimiting the Temperature, *Nucl. Phys. A* 408 (1983) 478–494. [doi:10.1016/0375-9474\(83\)90241-5](#).
- [46] P. Huovinen, P. Petreczky, Hadron resonance gas with repulsive interactions and fluctuations of conserved charges, *Phys. Lett. B* 777 (2018) 125–130. [arXiv:1708.00879](#), [doi:10.1016/j.physletb.2017.12.001](#).
- [47] P. Huovinen, P. Petreczky, Hadron resonance gas with repulsive interactions, *J. Phys. Conf. Ser.* 1070 (1) (2018) 012004. [doi:10.1088/1742-6596/1070/1/012004](#).
- [48] S. Pal, G. Kadam, A. Bhattacharyya, Hadron resonance gas model with repulsive mean-field interactions: Specific heat, isothermal compressibility and speed of sound, *Nucl. Phys. A* 1023 (2022) 122464. [arXiv:2104.08531](#), [doi:10.1016/j.nuclphysa.2022.122464](#).
- [49] S. Pal, G. Kadam, H. Mishra, A. Bhattacharyya, Effects of hadronic repulsive interactions on the fluctuations of conserved charges, *Phys. Rev. D* 103 (5) (2021) 054015. [arXiv:2010.10761](#), [doi:10.1103/PhysRevD.103.054015](#).
- [50] S. Pal, G. Kadam, A. Bhattacharyya, Conserved charge fluctuations in the relativistic mean-field hadron resonance gas model: constraints on hadronic repulsive interactions (5 2023). [arXiv:2305.13212](#).

- [51] S. Capstick, N. Isgur, Baryons in a relativized quark model with chromodynamics, *Phys. Rev. D* 34 (9) (1986) 2809–2835. [doi:10.1103/physrevd.34.2809](https://doi.org/10.1103/physrevd.34.2809).
- [52] D. Ebert, R. N. Faustov, V. O. Galkin, Mass spectra and Regge trajectories of light mesons in the relativistic quark model, *Phys. Rev. D* 79 (2009) 114029. [arXiv:0903.5183](https://arxiv.org/abs/0903.5183), [doi:10.1103/PhysRevD.79.114029](https://doi.org/10.1103/PhysRevD.79.114029).
- [53] P. Alba, V. M. Sarti, J. Noronha-Hostler, P. Parotto, I. Portillo-Vazquez, C. Ratti, J. M. Stafford, Influence of hadronic resonances on the chemical freeze-out in heavy-ion collisions, *Phys. Rev. C* 101 (5) (2020) 054905. [arXiv:2002.12395](https://arxiv.org/abs/2002.12395), [doi:10.1103/PhysRevC.101.054905](https://doi.org/10.1103/PhysRevC.101.054905).
- [54] J. Sollfrank, P. Huovinen, M. Kataja, P. V. Ruuskanen, M. Prakash, R. Venugopalan, Hydrodynamical description of 200-A/GeV/c S + Au collisions: Hadron and electromagnetic spectra, *Phys. Rev. C* 55 (1997) 392–410. [arXiv:nucl-th/9607029](https://arxiv.org/abs/nucl-th/9607029), [doi:10.1103/PhysRevC.55.392](https://doi.org/10.1103/PhysRevC.55.392).
- [55] A. Bazavov, et al., Skewness, kurtosis, and the fifth and sixth order cumulants of net baryon-number distributions from lattice QCD confront high-statistics STAR data, *Phys. Rev. D* 101 (7) (2020) 074502. [arXiv:2001.08530](https://arxiv.org/abs/2001.08530), [doi:10.1103/PhysRevD.101.074502](https://doi.org/10.1103/PhysRevD.101.074502).
- [56] A. Bazavov, et al., The chiral and deconfinement aspects of the QCD transition, *Phys. Rev. D* 85 (2012) 054503. [arXiv:1111.1710](https://arxiv.org/abs/1111.1710), [doi:10.1103/PhysRevD.85.054503](https://doi.org/10.1103/PhysRevD.85.054503).
- [57] C. Aubin, C. Bernard, C. DeTar, J. Osborn, S. Gottlieb, E. B. Gregory, D. Toussaint, U. M. Heller, J. E. Hetrick, R. Sugar, Light hadrons with improved staggered quarks: Approaching the continuum limit, *Phys. Rev. D* 70 (2004) 094505. [arXiv:hep-lat/0402030](https://arxiv.org/abs/hep-lat/0402030), [doi:10.1103/PhysRevD.70.094505](https://doi.org/10.1103/PhysRevD.70.094505).
- [58] Y. Aoki, et al., FLAG Review 2021, *Eur. Phys. J. C* 82 (10) (2022) 869. [arXiv:2111.09849](https://arxiv.org/abs/2111.09849), [doi:10.1140/epjc/s10052-022-10536-1](https://doi.org/10.1140/epjc/s10052-022-10536-1).
- [59] A. Bazavov, et al., Results for light pseudoscalar mesons, *PoS LATTICE2010* (2010) 074. [arXiv:1012.0868](https://arxiv.org/abs/1012.0868), [doi:10.22323/1.105.0074](https://doi.org/10.22323/1.105.0074).
- [60] T. Schäfer, F. Wilczek, Continuity of quark and hadron matter, *Phys. Rev. Lett.* 82 (1999) 3956–3959. [arXiv:hep-ph/9811473](https://arxiv.org/abs/hep-ph/9811473), [doi:10.1103/PhysRevLett.82.3956](https://doi.org/10.1103/PhysRevLett.82.3956).
- [61] A. Bazavov, et al., Chiral crossover in QCD at zero and non-zero chemical potentials, *Phys. Lett. B* 795 (2019) 15–21. [arXiv:1812.08235](https://arxiv.org/abs/1812.08235), [doi:10.1016/j.physletb.2019.05.013](https://doi.org/10.1016/j.physletb.2019.05.013).
- [62] A. Andronic, P. Braun-Munzinger, K. Redlich, J. Stachel, Decoding the phase structure of QCD via particle production at high energy, *Nature* 561 (7723) (2018) 321–330. [arXiv:1710.09425](https://arxiv.org/abs/1710.09425), [doi:10.1038/s41586-018-0491-6](https://doi.org/10.1038/s41586-018-0491-6).
- [63] S. Borsanyi, Z. Fodor, J. N. Guenther, R. Kara, S. D. Katz, P. Parotto, A. Pasztor, C. Ratti, K. K. Szabo, QCD Crossover at Finite Chemical Potential from Lattice Simulations, *Phys. Rev. Lett.* 125 (5) (2020) 052001. [arXiv:2002.02821](https://arxiv.org/abs/2002.02821), [doi:10.1103/PhysRevLett.125.052001](https://doi.org/10.1103/PhysRevLett.125.052001).
- [64] C. Bonati, M. D’Elia, F. Negro, F. Sanfilippo, K. Zambello, Curvature of the pseudocritical line in QCD: Taylor expansion matches analytic continuation, *Phys. Rev. D* 98 (5) (2018) 054510. [arXiv:1805.02960](https://arxiv.org/abs/1805.02960), [doi:10.1103/PhysRevD.98.054510](https://doi.org/10.1103/PhysRevD.98.054510).
- [65] R. Bellwied, S. Borsanyi, Z. Fodor, J. Günther, S. D. Katz, C. Ratti, K. K. Szabo, The QCD phase diagram from analytic continuation, *Phys. Lett. B* 751 (2015) 559–564. [arXiv:1507.07510](https://arxiv.org/abs/1507.07510), [doi:10.1016/j.physletb.2015.11.011](https://doi.org/10.1016/j.physletb.2015.11.011).
- [66] C. Bonati, M. D’Elia, M. Mariti, M. Mesiti, F. Negro, F. Sanfilippo, Curvature of the chiral pseudocritical line in QCD: Continuum extrapolated results, *Phys. Rev. D* 92 (5) (2015) 054503. [arXiv:1507.03571](https://arxiv.org/abs/1507.03571), [doi:10.1103/PhysRevD.92.054503](https://doi.org/10.1103/PhysRevD.92.054503).
- [67] A. Abhishek, S. Sharma, Towards a universal description of hadronic phase of QCD (3 2023). [arXiv:2303.03994](https://arxiv.org/abs/2303.03994).
- [68] T. M. Schwarz, S. P. Klevansky, G. Papp, The Phase diagram and bulk thermodynamical quantities in the NJL model at finite temperature and density, *Phys. Rev. C* 60 (1999) 055205. [arXiv:nucl-th/9903048](https://arxiv.org/abs/nucl-th/9903048), [doi:10.1103/PhysRevC.60.055205](https://doi.org/10.1103/PhysRevC.60.055205).
- [69] J. Randrup, J. Cleymans, Maximum freeze-out baryon density in nuclear collisions, *Phys. Rev. C* 74 (2006) 047901. [arXiv:hep-ph/0607065](https://arxiv.org/abs/hep-ph/0607065), [doi:10.1103/PhysRevC.74.047901](https://doi.org/10.1103/PhysRevC.74.047901).
- [70] J. Cleymans, H. Oeschler, K. Redlich, S. Wheaton, Transition from baryonic to mesonic freeze-out, *Phys. Lett. B* 615 (2005) 50–54. [arXiv:hep-ph/0411187](https://arxiv.org/abs/hep-ph/0411187), [doi:10.1016/j.physletb.2005.03.074](https://doi.org/10.1016/j.physletb.2005.03.074).
- [71] J. Cleymans, K. Redlich, Unified description of freezeout parameters in relativistic heavy ion collisions, *Phys. Rev. Lett.* 81 (1998) 5284–5286. [arXiv:nucl-th/9808030](https://arxiv.org/abs/nucl-th/9808030), [doi:10.1103/PhysRevLett.81.5284](https://doi.org/10.1103/PhysRevLett.81.5284).
- [72] A. Motornenko, J. Steinheimer, V. Vovchenko, S. Schramm, H. Stoecker, Equation of state for hot QCD and compact stars from a mean field approach, *Phys. Rev. C* 101 (3) (2020) 034904. [arXiv:1905.00866](https://arxiv.org/abs/1905.00866), [doi:10.1103/PhysRevC.101.034904](https://doi.org/10.1103/PhysRevC.101.034904).